https://doi.org/10.1016/j.applthermaleng.2017.06.020

Mathematical modeling of direct formate fuel cells

L. An[a]* and R. Chen[b,c]*

[a] Department of Mechanical Engineering, The Hong Kong Polytechnic University, Hung Hom, Kowloon, Hong Kong SAR, China

[b] Key Laboratory of Low-grade Energy Utilization Technologies and Systems (Chongqing University), Ministry of Education, Chongqing 400030, China

[c] Institute of Engineering Thermophysics, Chongqing University, Chongqing 400030, China

*Corresponding authors.

[a] Tel.: 852-27667820; fax: 852-23654703; e-mail: liang.an@polyu.edu.hk (L. An)

[b,c] Tel.: 86-23-65102474; fax: 86-23-65102474; e-mail: rchen@cqu.edu.cn (R. Chen)

Abstract

In this work, we develop a one-dimensional mathematical model for direct formate fuel cells (DFFC), which incorporates transport and electrochemical processes. The present model is validated against literature experimental results and it shows good agreement. In addition, we also investigate effects of operating and structural parameters on the cell voltage. Results exhibit that the cell voltage is increased with the reactant concentration, including formate, hydroxide ions, and oxygen, which originates from the reduced activation polarization and concentration polarization. Moreover, it is also shown that increasing the exchange current density much reduces electrode overpotentials and thus upgrades the cell performance. The model is further used to examine how the anode diffusion layer and the membrane affect the cell performance. It is found that the cell performance is upgraded with increasing the porosity of the anode diffusion layer and decreasing the thickness of the anode

diffusion layer or membrane.

Keywords: Fuel cell; Direct formate fuel cell; Mathematical modeling; Mass transport; Polarization

1. Introduction

Direct liquid fuel cells (DLFC) have recently attracted worldwide attention, primarily because liquid fuels possess obvious advantages over gaseous hydrogen in terms of transportation, storage, as well as handling [1-8]. Among various liquid fuels, formate has recently received ever-increasing attention, primarily because formate salts are readily stored, transported, and handled in their solid state and can be easily dissolved into water to form a liquid fuel [9-17]. Recently, it has been demonstrated that, adding an alkali (e.g.: NaOH/KOH) to the fuel solution would much improve the fuel cell performance [18-20]. Such an improvement can be attributed to the involvement of an alkali, which not only dramatically increases the ionic conductivity of hydroxide exchange membranes (HEM) [21, 22], but also enables the electrochemical kinetics of the formate oxidation reaction (FOR) to be further enhanced [23, 24]. It should be noted that the presence of both Na^+/K^+ ions and OH^- ions in the fuel cell system creates an anion-cation co-existing system, thereby showing more complicated physicochemical processes [25], including mass transport, ion transport, electron transport, and electrochemical reactions. On the other hand, the direct formate fuel cell (DFFC) has a complex multi-layered porous structure, in which the transport and electrochemical processes occur simultaneously. Hence, it is hard to shed light on the complicated processes via experimental investigations. Alternatively, the mathematical modeling plays an important role in quantifying the transport and electrochemical processes in fuel cells. To our best knowledge, there is no attempt to mathematically investigate the DFFC. In this work, a mathematical model is developed for the DFFC and effects of design and operating parameters on the cell performance are examined.

2. Formulation

Fig. 1 shows a DFFC configuration that is comprised of a membrane electrode assembly (MEA) clamped between two bipolar plates, which sequentially includes an anode diffusion layer (DL), an anode catalyst layer (CL), an HEM, a cathode CL, and a cathode DL. On the anode, the formate in the fuel solution is oxidized to produce electrons, water, and carbonate ions according to Ref. [26]:

$$HCOO^- + 3OH^- \rightarrow CO_3^{2-} + 2H_2O + 2e^- \qquad E_a^0 = -1.05V \qquad (1)$$

On the cathode, oxygen reduction reaction (ORR) happens to generate hydroxide ions according to Refs. [27, 28]:

$$\tfrac{1}{2}O_2 + H_2O + 2e^- \rightarrow 2OH^- \qquad E_c^0 = 0.40V \qquad (2)$$

The combination of the FOR and the ORR results in an overall reaction:

$$HCOO^- + \tfrac{1}{2}O_2 + OH^- \rightarrow CO_3^{2-} + H_2O \qquad E^0 = 1.45V \qquad (3)$$

This theoretical voltage is higher than those of fuel cells running on other liquid fuels, such as methanol (1.23 V) and ethanol (1.14 V) [29, 30].

To simplify the complicated processes, a one-dimensional model is developed with the following simplifications and assumptions:

(1) The fuel cell operations are under steady-state condition.

(2) The transport through DLs is assumed to be a diffusion-predominated process.

(3) As CL is much thinner than DL; hence, CL is treated as an interface.

(4) Since there is no mixed-potential phenomenon in this fuel cell system, the formate crossover through the HEM is ignored.

2.1. Transport model

As mentioned earlier, there is no electrochemical reaction occurring in the anode DL. Hence, the mass conservation of reactants/products in the anode DL can be

expressed as [31]:

$$\nabla N_i = 0 \tag{4}$$

where *i* represents $HCOO^-$, OH^-, or CO_3^{2-}. As mass/charge transport through the anode DL is considered to be a diffusion-predominated process, the flux (N_i) can be written based on Fick's law:

$$N_i = -D_i^{eff} \frac{dC_i}{dx} \tag{5}$$

in which *C* denotes the reactant/product concentration, and the effective diffusivity, D_i^{eff}, (*i*: $HCOO^-$, OH^-, or CO_3^{2-}) is given by:

$$D_i^{eff} = \varepsilon^{3/2} D_i \tag{6}$$

where D_i and ε represents the diffusivity of the reactant/product and the porosity of the anode DL, respectively. The electroneutrality of the fuel solution in the anode DL is followed by [32]:

$$\sum_i z_i C_i = 0 \tag{7}$$

where *z* stands for the valence of ions and *i* denotes $HCOO^-$, Na^+/K^+, OH^- or CO_3^{2-}.

On the cathode, the air or pure oxygen can be employed as oxidant in this fuel cell system. For the case of the fuel cell using the air, oxygen extracted from the air reacts with electrons and water to generate the hydroxide ions in the cathode CL. Similarly, the mass conservation of oxygen in the cathode DL is expressed as [33]:

$$\nabla N_{O_2} = 0 \tag{8}$$

Then, the oxygen flux (N_{O_2}) can be expressed based on Fick's law:

$$N_{O_2} = -D_{O_2}^{eff} \frac{dC_{O_2}}{dx} \tag{9}$$

where the effective diffusivity ($D_{O_2}^{eff}$) is given by:

$$D_{O_2}^{eff} = \varepsilon^{3/2} D_{O_2} \tag{10}$$

For the case of using pure oxygen on the cathode, it is assumed that the cathode is fully filled by pure oxygen.

2.2. Electrochemical model

The formate oxidation mechanisms in alkaline media have been extensively investigated [34-36]. The previous studies showed the formate oxidation in alkaline media is a complicated electrochemical process, and the mechanism is not completely understood. To simplify the electrochemical process, a Tafel-form electrochemical model for the electro-oxidation of formate incorporating the mass-transfer effect is applied:

$$j_a = i_{0,a} \left(\frac{C_{HCOO^-}^{ACL}}{C_{HCOO^-}^{ref}}\right)^{\gamma_a^{HCOO^-}} \left(\frac{C_{OH^-}^{ACL}}{C_{OH^-}^{ref}}\right)^{\gamma_a^{OH^-}} \exp\left(\frac{\alpha_a F}{RT}\eta_a\right) \tag{11}$$

$$\gamma_a^{HCOO^-} = \begin{cases} 0 & C_{HCOO^-}^{ACL} > C_{HCOO^-}^{ref} \\ 1 & C_{HCOO^-}^{ACL} \le C_{HCOO^-}^{ref} \end{cases} \tag{12}$$

$$\gamma_a^{OH^-} = \begin{cases} 0 & C_{OH^-}^{ACL} > C_{OH^-}^{ref} \\ 1 & C_{OH^-}^{ACL} \le C_{OH^-}^{ref} \end{cases} \tag{13}$$

where C_i^{ACL} is the reactant concentration in the anode CL and C_i^{ref} is the reference concentration of reactant. The reaction order γ is related to the species concentration and is assumed to be zero-order when its concentration is higher than a reference value. Otherwise, a first-order reaction is specified.

Similarly, a Tafel-form electrochemical model is also employed for the electro-reduction of oxygen in alkaline media:

$$j_c = i_{0,c} \left(\frac{C_{O_2}^{CCL}}{C_{O_2}^{ref}}\right)^{\gamma_c} \exp\left(\frac{\alpha_c F}{RT}\eta_c\right) \tag{14}$$

$$\gamma_c = \begin{cases} 0 & C_{O_2}^{CCL} > C_{O_2}^{ref} \\ 1 & C_{O_2}^{CCL} \le C_{O_2}^{ref} \end{cases} \quad (15)$$

where $C_{O_2}^{CCL}$ is the oxygen concentration in the cathode CL and $C_{O_2}^{ref}$ is the reference concentration of oxygen.

2.3. Boundary conditions

On the anode,

$x = x_1$: $C_i = C_i^{inlet}$ (i: $HCOO^-$, Na^+/K^+, OH^-, or CO_3^{2-}) (16)

$x = x_2$: $N_i = \frac{i_{cell} s_i}{n_a F}$ (i: $HCOO^-$, OH^-, or CO_3^{2-}) (17)

On the cathode,

$x = x_3$: $N_{O_2} = \frac{i_{cell} s_{O_2}}{n_c F}$ (18)

$x = x_4$: $C_{O_2} = C_{O_2}^{inlet}$ (19)

2.4. Cell voltage

With the results obtained from the above-mentioned equations, the cell voltage can be determined [37]:

$$V_{cell} = E^0 - \eta_a - \eta_c - i_{cell}(R_{contact} + \frac{\delta_M}{\sigma_M}) \quad (20)$$

where E^0 is the theoretical voltage, and the total cell resistance is attributed to the contact resistance ($R_{contact}$) and membrane resistance ($\frac{\delta_M}{\sigma_M}$). In addition, the physicochemical, operating, structural and transport parameters are presented in Tables 1-4, respectively.

3. Results and discussion

3.1. Model validation

The numerical results and literature experimental data are compared and presented in Fig. 2. The experimental data were collected when the fuel cell was operated at

60°C with a fuel solution (2.0 M formate + 2.0 M KOH) and pure oxygen [38]. It can be seen that the predicted curve is in good agreement with the experimental data in the open literature. Fig. 3 specifies the anode polarization, cathode polarization and the ohmic polarization from the overall polarization curve. It is the fact that the anode/cathode polarization is attributed to the activation polarization (electrochemical loss) and the concentration polarization (transport loss), while the ohmic polarization is associated with the charge conduction (electron and ion) [18]. It is found that the largest polarization appears on the anode, indicating that the major loss in the DFFC results from the anode polarization. In the following sections, the numerical results on how various design and operating parameters affect the cell performance will be presented.

3.2. Effect of the formate concentration

For a given fuel cell design, the formate concentration in the fuel solution becomes an important parameter to achieve an appropriate formate concentration in the anode CL. Hence, the effect of the formate concentration on the cell performance is investigated and presented in Fig. 4a. It is shown that an increase in the formate concentration from 0.5 M to 2.0 M increases the cell voltage. It is clear that the improvement in cell performance is attributed to two aspects: (1) an increase in the formate concentration will enhance the electrochemical kinetics of the FOR, which can be evident from the anode overpotential shown in Fig. 4b; and (2) increasing the formate concentration means increasing the delivery rate of formate to the anode CL, which can be evident from the local concentration of formate shown in Fig. 4c. Too low local concentration of formate has the large activation polarization at low current densities and the large concentration polarization at high current densities, as shown in Figs. 4b and 4c. For example, the limiting current density is increased from 870 A

m^{-2} to 3500 A m^{-2} when the formate concentration increases from 0.5 M to 2.0 M. Therefore, an increase in the formate concentration from 0.5 M to 2.0 M improves cell performance.

3.3. Effect of the hydroxide-ion concentration

Presently, an alkali has to be added into the fuel solution because the ionic conductivity of state-of-the-art HEMs is rather low. On the other hand, the addition of an alkali is found to further enhance the electrochemical kinetics of the FOR. Hence, the effect of the hydroxide-ion concentration is examined and the numerical results are presented in Fig. 5. As expected, increasing the hydroxide-ion concentration increases the cell voltage. For example, at 2000 A m^{-2}, the cell voltage increases from 0.401 V to 0.545 V when the hydroxide-ion concentration increases from 0.5 M to 2.0 M. This is because an increase in the hydroxide-ion concentration not only improves the electrochemical kinetics of the FOR (see Fig. 5b), but also increases the delivery rate of hydroxide ions (see Fig. 5c). It is noted from Fig. 5 that too low hydroxide-ion concentration will cause the large activation polarization at low current densities and the large concentration polarization at high current densities. For example, it is seen from Fig. 5a that the limiting current density appears for the case of the 0.5-M operation, which is caused by the mass-transport limitation of hydroxide-ion ions, which can be evident from the local concentration of hydroxide ion shown in Fig. 5c. It should be mentioned that although other three operations (1.0-M, 1.5-M and 2.0-M) also show the limiting current densities, but those mass-transport limitations are caused by the formate, rather than the hydroxide ion, which can be evident from the local concentrations of formate and hydroxide ion shown in Figs. 4c and 5c.

3.4. Effect of the oxygen concentration

In practice, the air is generally used as oxidant even though the pre-removal of

carbon dioxide is needed for alkaline fuel cells. Hence, the fuel cell using the air is examined and the comparison with that using pure oxygen is presented in Fig. 6. It is found that the fuel cell using the air increases the cathode overpotential and thus decreases the cell voltage, which is consistent with the previous investigations [39]. For example, at 2000 A m^{-2}, the cell voltage decreases from 0.545 V to 0.470 V when the oxidant is changed from pure oxygen to the air, as shown in Fig. 6a. The higher oxygen concentration results in a faster electrochemical kinetics of the ORR and thus a lower activation polarization, as shown in Fig. 6b. For the case of using the air as oxidant, oxygen is transported from the cathode flow field through the cathode DL to the cathode CL, where the oxygen concentration becomes lower due to the consumption by the ORR. However, the previous study has shown that the decrease in the oxygen concentration from the flow field to the CL is rather small, resulting from the fast delivery rate of oxygen in its intrinsic gas state [31]. Therefore, it is suggested that the oxygen delivery rate is high enough to match the reaction rate.

3.5. Effect of the exchange current density

As a result of the fact that the exchange current densities on the anode and cathode can significantly affect the anode and cathode overpotentials, respectively, the effect of the respective exchange current density is examined and presented in Figs. 7 and 8. An increase in the exchange current density dramatically reduces the overpotentials (Figs. 7b and 8b) and thus improves the cell voltage (Figs. 7a and 8a). For example, at 2000 A m^{-2}, the cell voltage increases from 0.545 V to 0.695 V when the anodic exchange current density is increased from 10 A m^{-2} to 100 A m^{-2}, as shown in Fig. 7a. In addition, it is also shown that the cell voltage increases from 0.364 V to 0.545 V when the cathodic exchange current density is increased from 1 A m^{-2} to 44 A m^{-2}, as shown in Fig. 8a. Therefore, it is critically important to develop highly active

electrocatalysts to increase the exchange current densities of the formate oxidation and oxygen reduction reactions.

3.6. Effect of the membrane thickness

Due to the fact that the fast kinetics rendered by the alkaline environment allows us to use the non-precious-metal catalysts on the cathode, most of them are inactive to the crossovered fuels, dramatically alleviating the mixed-pontifical problem and thus enabling the use of the thin membrane. Typically, the membrane thickness can range from 28 μm (Tokuyama A201) to 125 μm (Nafion115). The effect of the membrane thickness is investigated and presented in Fig. 9. The voltage is found to slightly decrease with increasing the membrane thickness at high current densities. For example, at 2000 A m^{-2}, the cell voltage decreases from 0.545 V to 0.511 V when the membrane thickness is increased from 28 μm to 120 μm, as shown in Fig. 9. Although the thinner membrane is preferred from power output point of view, a thinner membrane means the higher fuel crossover rate, definitely decreasing the fuel utilization efficiency, and the worse mechanical property. Hence, the positive effect of the low ohmic polarization and the negative effect of the high fuel crossover rate and the poor mechanical property will result in an optimal thickness for the membrane selection.

3.7. Effect of the anode structural design parameters

As mentioned earlier, formate in the fuel solution is transported through the anode DL to the anode CL. Hence, the structural design parameters can affect the transport process of formate. For this reason, the effects of the anode DL thickness and porosity on the cell performance are also investigated. It can be seen from Fig. 10 that an increase in the anode DL thickness from 50 μm to 200 μm decreases the cell voltage. This is because the thicker DL increases the mass-transport resistance of

reactants/products. As for the anode DL porosity, it is shown that increasing the porosity from 0.7 to 0.9 increases the cell voltage, particularly at high current densities, as shown in Fig. 11. This is due to the fact that larger porosity has a higher mass-transport rate. For this reason, the DL with a large porosity is preferred from mass-transport point of view; for example, the nickel foam with a porosity of 95% is generally used as the DL in alkaline direct ethanol fuel cells [40]. In addition, there are three functions for the DL in fuel cells, i.e., a reactant distributor, an electron transmitter, and a CL supporter [31]. On the other hand, a porous structure with a larger porosity means a larger electron transport resistance and the worse mechanical property. In practice, therefore, there will be an optimal value for the DL porosity by simultaneously considering the positive and negative effects.

4. Concluding remarks

We have developed a mathematical model for direct formate fuel cells by incorporating the transport and electrochemical processes simultaneously occurring. The numerical results are in good agreement with the experimental data in the open literature. It is found that the major voltage loss results from the anode polarization. As expected, the voltage is increased with the reactant concentration, including formate, hydroxide-ion and oxygen, primarily due to the decreased activation polarization and the increased mass-transport rate. In addition, it is also shown that the respective exchange current density has a significant influence on the performance. Furthermore, the performance is upgraded with an increase in the anode DL porosity, but with a decrease in the anode DL thickness and the membrane thickness.

Acknowledgements

The authors gratefully acknowledge the financial supports of the Natural Science Foundation of China (No. 51506039 and No. 51576021).

References

[1] L. An, R. Chen, Recent progress in alkaline direct ethylene glycol fuel cells for sustainable energy production, J. Power Sources 329 (2016) 484-501.

[2] L. An, T.S. Zhao, J.B. Xu, A bi-functional cathode structure for alkaline-acid direct ethanol fuel cells, Int. J. Hydrogen Energy 36 (2011) 13089-13095.

[3] L. An, T.S. Zhao, Y.S. Li, Carbon-neutral sustainable energy technology: Direct ethanol fuel cells, Renewable and Sustainable Energy Reviews 50 (2015) 1462-1468.

[4] E. Antolini, E.R. Gonzalez, Alkaline direct alcohol fuel cells, J. Power Sources 195 (2010) 3431-3450.

[5] L. An, T.S. Zhao, S.Y. Shen, Q.X. Wu, R. Chen, An alkaline direct oxidation fuel cell with non-platinum catalysts capable of converting glucose to electricity at high power output, J. Power Sources 196 (2011) 186-190.

[6] L. An, T.S. Zhao, X.H. Yan, X.L. Zhou, P. Tan, The dual role of hydrogen peroxide in fuel cells, Science Bulletin 60 (2015) 55-64.

[7] B. Wang, Y. Zhou, Q. Du, Y. Yin, K. Jiao, Transient investigation of passive alkaline membrane direct methanol fuel cell, Applied Thermal Engineering 100 (2016) 1245-1258.

[8] I. Verhaert, S. Verhelst, H. Huisseune, I. Poels, G. Janssen, G. Mulder, M. De Paepe, Thermal and electrical performance of an alkaline fuel cell, Applied Thermal Engineering 40 (2012) 227-235.

[9] Y.S. Li, Y.L. He, W.W. Yang, A high-performance direct formate-peroxide fuel cell with palladium-gold alloy coated foam electrodes, J. Power Sources 278 (2015)

569-573.

[10] K. Tran, T.Q. Nguyen, A.M. Bartrom, A. Sadiki, J.L. Haan, A fuel-flexible alkaline direct liquid fuel cell, Fuel Cells 14 (2014) 834-841.

[11] T.Q. Nguyen, D. Minami, C. Hua, A. Miller, K. Tran, J.L. Haan, Ambient temperature operation of a platinum-free direct formate fuel cell, Journal of Fuel Cell Science and Technology 12 (2015) 1-4.

[12] L. An, T.S. Zhao, Transport phenomena in alkaline direct ethanol fuel cells for sustainable energy production, J. Power Sources 341 (2017) 199-211.

[13] Y.S. Li, Y. Feng, X.D. Sun, Y.L. He, A sodium-ion-conducting direct formate fuel cell: generating electricity and producing base, Angew. Chem. Int. Ed. 56 (2017) 5734-5737.

[14] Y.S. Li, X.D. Sun, Y. Feng, Hydroxide self-feeding high-temperature alkaline direct formate fuel cells, Chemsuschem DOI: 10.1002/cssc.201700228.

[15] G.L. Soloveichik, Liquid fuel cells, Beilstein Journal of Nanotechnology, 5 (2014) 1399-1418.

[16] L. An, T.S. Zhao, L. Zeng, Agar chemical hydrogel electrode binder for fuel-electrolyte-fed fuel cells, Applied Energy 109 (2013) 67-71.

[17] S.J. Wang, W.W. Huo, Z.Q. Zou, Y.J. Qiao, H. Yang, Computational simulation and experimental evaluation on anodic flow field structures of micro direct methanol fuel cells, Applied Thermal Engineering 31 (2011) 2877-2884.

[18] L. An, T.S. Zhao, S.Y. Shen, Q.X. Wu, R. Chen, Performance of a direct ethylene glycol fuel cell with an anion-exchange membrane, Int. J. Hydrogen Energy 35 (2010) 4329-4335.

[19] L. An, T.S. Zhao, An alkaline direct ethanol fuel cell with a cation exchange membrane, Energy Environ. Sci. 4 (2011) 2213-2217.

[20] L. An, T.S. Zhao, L. Zeng, X.H. Yan, Performance of an alkaline direct ethanol fuel cell with hydrogen peroxide as oxidant, Int. J. Hydrogen Energy 39 (2014) 2320-2324.

[21] E. Agel, J. Bouet, J.F. Fauvarque, Characterization and use of anionic membranes for alkaline fuel cells, J. Power Sources 101 (2001) 267-274.

[22] L. An, T.S. Zhao, Q.X. Wu, L. Zeng, Comparison of different types of membrane in alkaline direct ethanol fuel cells, Int. J. Hydrogen Energy 37 (2012) 14536-14542.

[23] A.M. Bartrom, J. Ta, T.Q. Nguyen, J. Her, A. Donovan, J.L. Haan, Optimization of an anode fabrication method for the alkaline direct formate fuel cell, J. Power Sources 229 (2013) 234-238.

[24] Y.S. Li, H. Wu, Y.L. He, Y. Liu, L. Jin, Performance of direct formate-peroxide fuel cells, J. Power Sources 287 (2015) 75-80.

[25] L. An, T.S. Zhao, Y.S. Li, Q.X. Wu, Charge carriers in alkaline direct oxidation fuel cells, Energy & Environmental Science 5 (2012) 7536-7538.

[26] Y.S. Li, A liquid-electrolyte-free anion-exchange membrane direct formate-peroxide fuel cell, Int. J. Hydrogen Energy 41 (2016) 3600-3604.

[27] L. An, R. Chen, Direct formate fuel cells: A review, J. Power Sources 320 (2016) 127-139.

[28] L. An, T.S. Zhao, R. Chen, Q.X. Wu, A novel direct ethanol fuel cell with high power density, J. Power Sources 196 (2011) 6219–6222.

[29] X.H. Yan, T.S. Zhao, L. An, G. Zhao, L. Shi, A direct methanol-hydrogen peroxide fuel cell with a Prussian Blue cathode, Int. J. Hydrogen Energy 41 (2016) 5135-5140.

[30] L. An, T.S. Zhao, X.L. Zhou, L. Wei, X.H. Yan, A high-performance ethanol-hydrogen peroxide fuel cell, RSC Adv. 4 (2014) 65031-65034.

346 [31] L. An, Z.H. Chai, L. Zeng, P. Tan, T.S. Zhao, Mathematical modeling of alkaline
347 direct ethanol fuel cells, Int. J. Hydrogen Energy 38 (2013) 14067 -14075.
348 [32] X.L. Zhou, T.S. Zhao, L. An, Y.K. Zeng, X.H. Yan, A vanadium redox flow
349 battery model incorporating the effect of ion concentrations on ion mobility, Applied
350 Energy 158 (2015) 157-166.
351 [33] R. Chen, T.S. Zhao, Mathematical modeling of a passive-feed DMFC with heat
352 transfer effect, J. Power Sources 152 (2005) 122-130.
353 [34] J. John, H. Wang, E.D. Rus, H.D. Abruña, Mechanistic studies of formate
354 oxidation on platinum in alkaline medium, J. Phys. Chem. C 116 (2012) 5810−5820.
355 [35] P.A. Christensen, A. Hamnett, D. Linares-Moya, The electro-oxidation of
356 formate ions at a polycrystalline Pt electrode in alkaline solution: an in situ FTIR
357 study, Phys. Chem. Chem. Phys. 13 (2011) 11739-11747.
358 [36] J.H. Jiang, J. Scott, A. Wieckowski, Direct evidence of a triple-path mechanism
359 of formate electrooxidation on Pt black in alkaline media at varying temperature. Part
360 I: The electrochemical studies, Electrochimica Acta 104 (2013) 124-133.
361 [37] W.W. Yang, T.S. Zhao, A two-dimensional, two-phase mass transport model for
362 liquid-feed DMFCs, Electrochimica Acta 52 (2007) 6125-6140.
363 [38] A.M. Bartrom, J.L. Haan, The direct formate fuel cell with an alkaline anion
364 exchange membrane, J. Power Sources 214 (2012) 68-74.
365 [39] L. An, L. Zeng, T.S. Zhao, An alkaline direct ethylene glycol fuel cell with an
366 alkali-doped polybenzimidazole membrane, Int. J. Hydrogen Energy 38 (2013)
367 10602-10606.
368 [40] L. An, T.S. Zhao, Performance of an alkaline-acid direct ethanol fuel cell, Int. J.
369 Hydrogen Energy 36 (2011) 9994–9999.
370 [41] P. Taberner, J. Hettbaum, W. Vielstich, The influence of the electrolyte

composition on the formate oxidation in alkaline formate-air fuel cells, Electrochimica Acta 21 (1976) 439-440.

[42] H. Bahrami, A. Faghri, Multi-layer membrane model for mass transport in a direct ethanol fuel cell using an alkaline anion exchange membrane. J. Power Sources 218 (2012) 286-96.

[43] http://fuelcellsetc.com/store/DS/gas-diffusion-layer-properties.pdf

[44] L. An, T.S. Zhao, Z.H. Chai, L. Zeng, P. Tan, Modeling of the mixed potential in hydrogen peroxide-based fuel cells, Int. J. Hydrogen Energy 39 (2014) 7407-7416.

[45] M. Flurry, T. Gimmi, Solute diffusion, In Methods of Soil Analysis, Part 4, Physical Methods, edited by J.H. Dane and G.C. Topp, pp. 1323-1351, Soil Science Society of America, Madison, WI, 2002.

Nomenclature

C	Concentration, mol m^{-3}

D	Diffusivity, $m^2\ s^{-1}$
E^0	Theoretical potential/voltage, V
F	Faraday's constant, $A\ s\ mol^{-1}$
i	Current density, $A\ m^{-2}$
i_0	Exchange current density, $A\ m^{-2}$
j	Transfer current density, $A\ m^{-2}$
N	Flux, $mol\ m^{-2}\ s^{-1}$
P	Gas pressure, Pa
R	Universal gas constant, $J\ mol^{-1}\ K^{-1}$
T	Operating temperature, K
x	Coordinate
z	Valence of ion

Greek

α	Transfer coefficient
δ	Thickness, m
ε	Porosity
γ	Reaction order
η	Overpotential, V
σ	Conductivity, $\Omega^{-1}\ m^{-1}$

Superscripts

ACL	Anode catalyst layer
CCL	Cathode catalyst layer
eff	Effective
$inlet$	Inlet
O_2	Oxygen
OH^-	Hydroxyl ion
ref	Reference

Subscripts

0	Standard
a	Anode
c	Cathode
CO_3^{2-}	Carbonate
$HCOO^-$	Formate
i	Species
M	Membrane
Na^+	Sodium ion
O_2	Oxygen
OH^-	Hydroxyl ion

Table captions

Table 1 Physicochemical parameters.

Table 2 Operating parameters.

Table 3 Structural parameters.

Table 4 Mass/charge transport parameters.

Figure captions

425 Fig. 1 Schematic of a direct formate fuel cell and the computational domain.

426 Fig. 2 Comparison between numerical results and literature experimental data [38].

427 Fig. 3 Specific polarizations at various current densities.

428 Fig. 4 Effect of the formate concentration on the cell performance: (a) polarization

429 curves; (b) anode overpotentials; and (c) local concentrations.

430 Fig. 5 Effect of the hydroxide-ion concentration on the cell performance: (a)

431 polarization curves; (b) anode overpotentials; and (c) local concentrations.

432 Fig. 6 Effect of the oxygen concentration on the cell performance: (a) polarization

433 curves and (b) cathode overpotentials.

434 Fig. 7 Effect of the anodic exchange current density on the cell performance: (a)

435 polarization curves and (b) anode overpotentials.

436 Fig. 8 Effect of the cathodic exchange current density on the cell performance: (a)

437 polarization curves and (b) anode overpotentials.

438 Fig. 9 Effect of the membrane thickness on the cell performance.

439 Fig. 10 Effect of the anode DL thickness on the cell performance: (a) polarization

440 curves and (b) anode overpotentials.

441 Fig. 11 Effect of the anode DL porosity on the cell performance: (a) polarization

442 curves and (b) anode overpotentials.

443

444

445

446

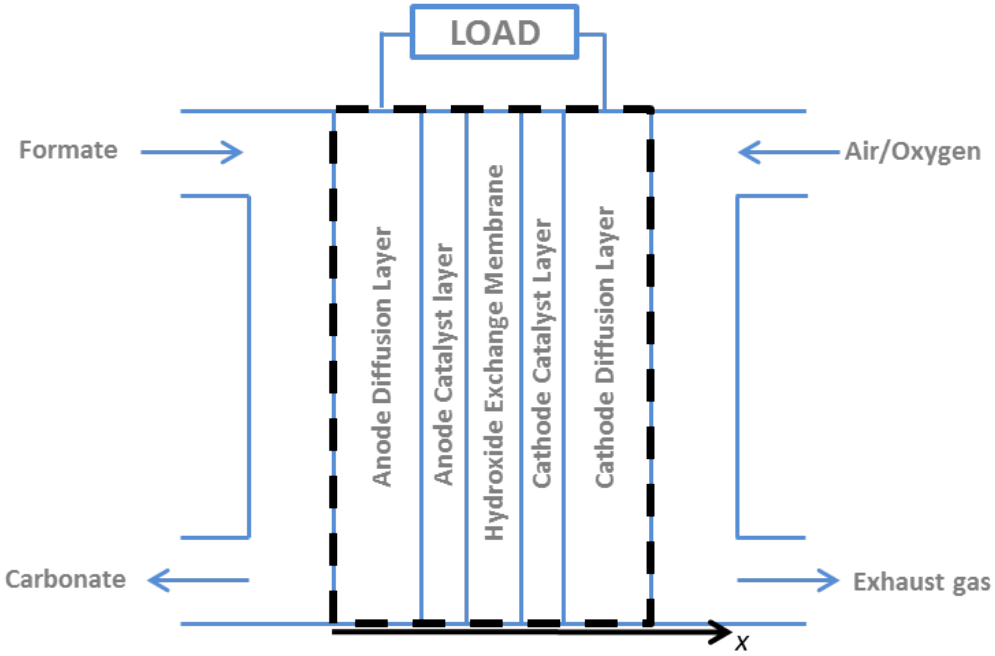

Fig. 1 Schematic of a direct formate fuel cell and the computational domain.

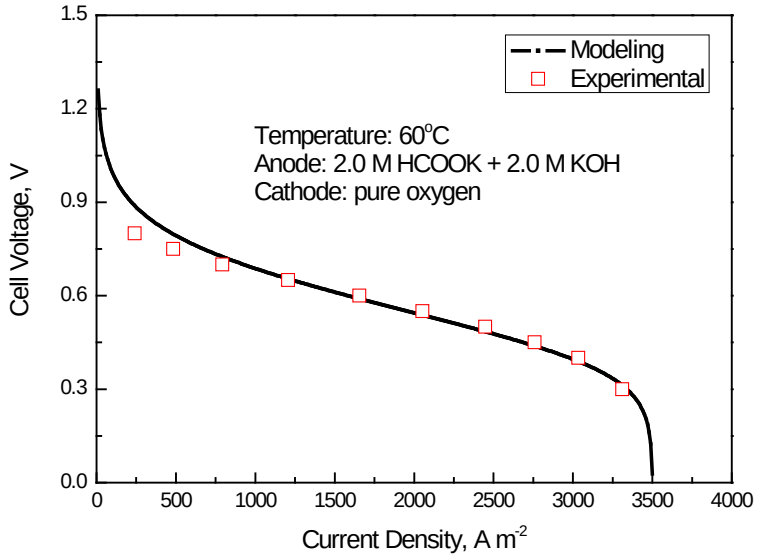

Fig. 2 Comparison between numerical results and literature experimental data [38].

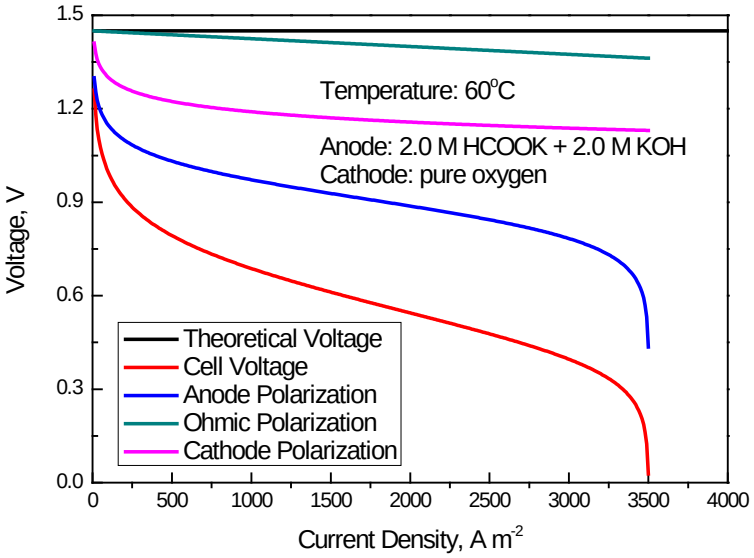

Fig. 3 Specific polarizations at various current densities.

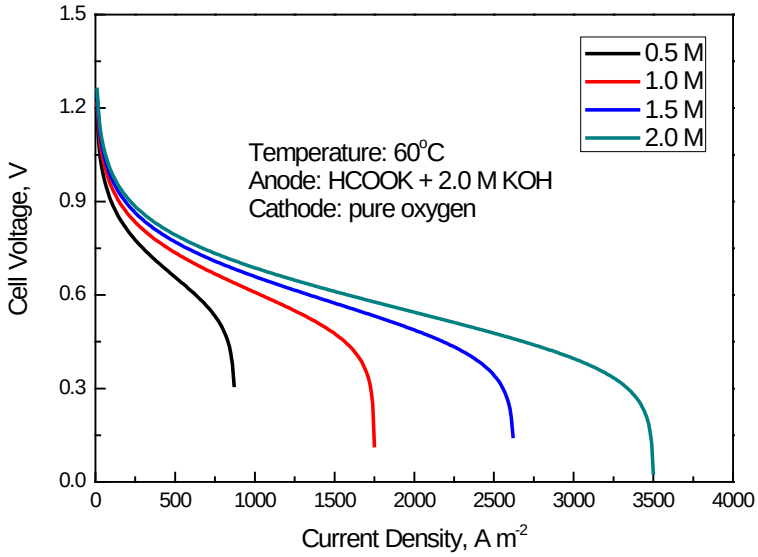

490

491 (a)

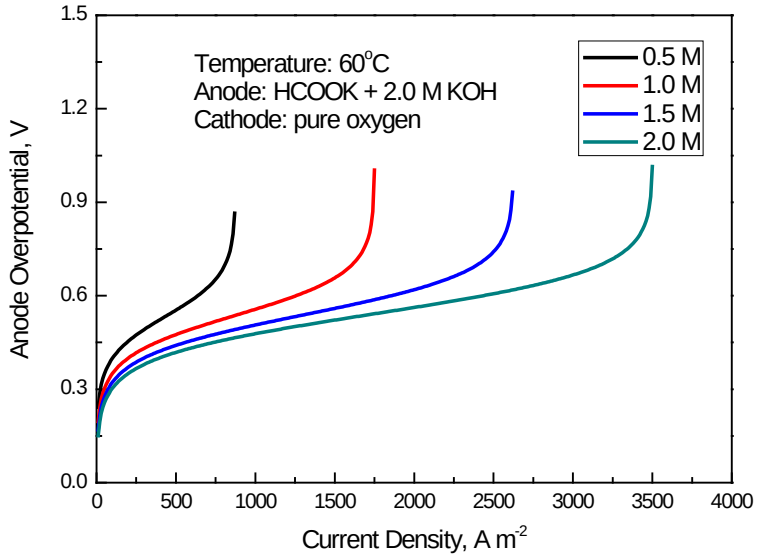

492

493 (b)

494

495

496

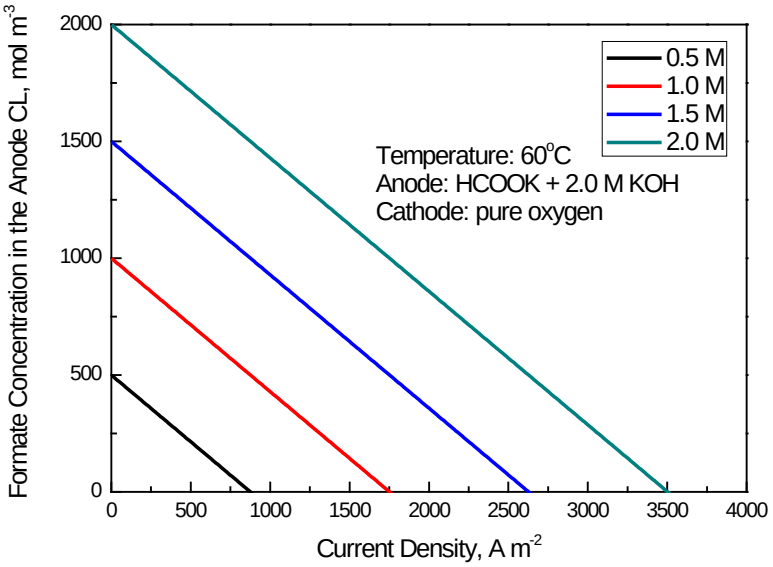

(c)

Fig. 4 Effect of the formate concentration on the cell performance: (a) polarization curves; (b) anode overpotentials; and (c) local concentrations.

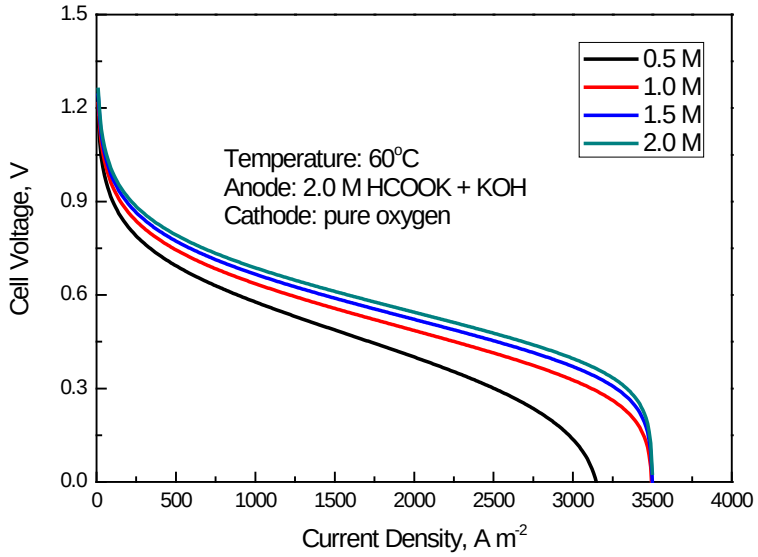

511

512 (a)

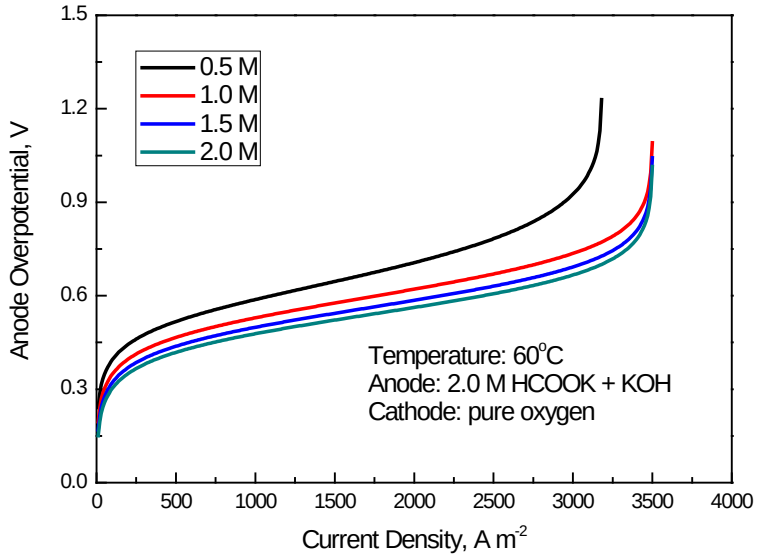

513

514 (b)

515

516

517

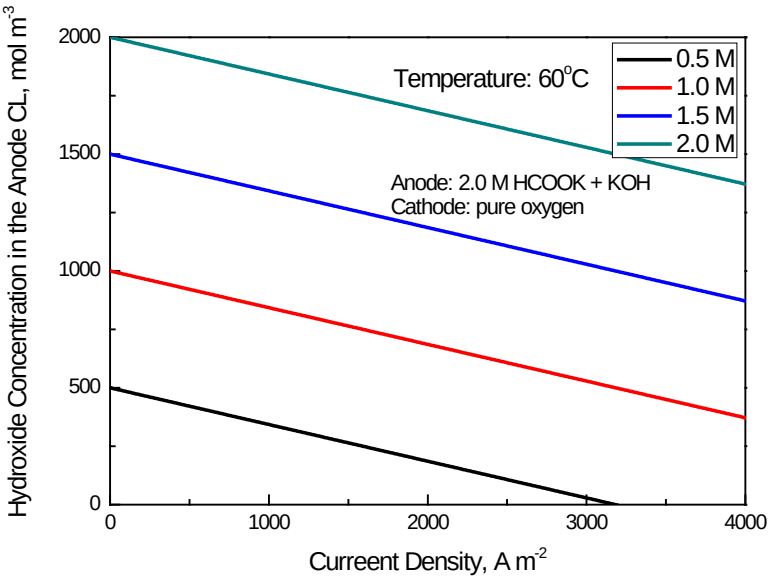

Fig. 5 Effect of the hydroxide-ion concentration on the cell performance: (a) polarization curves; (b) anode overpotentials; and (c) local concentrations.

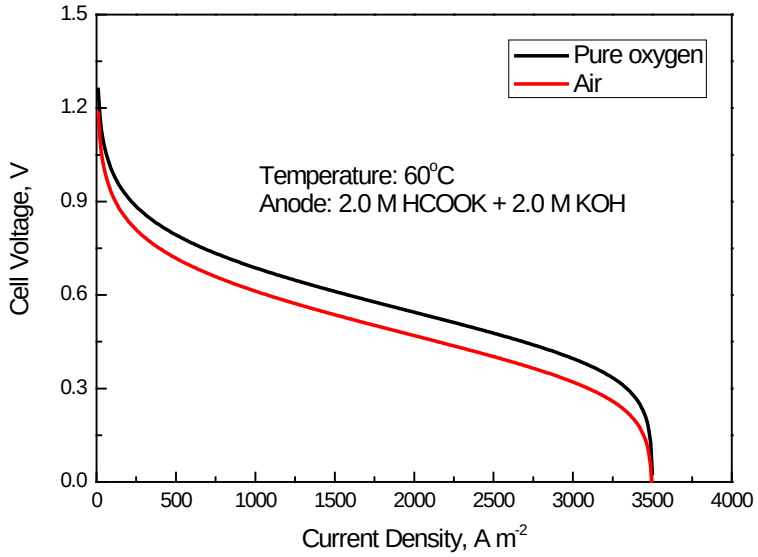

531

532 (a)

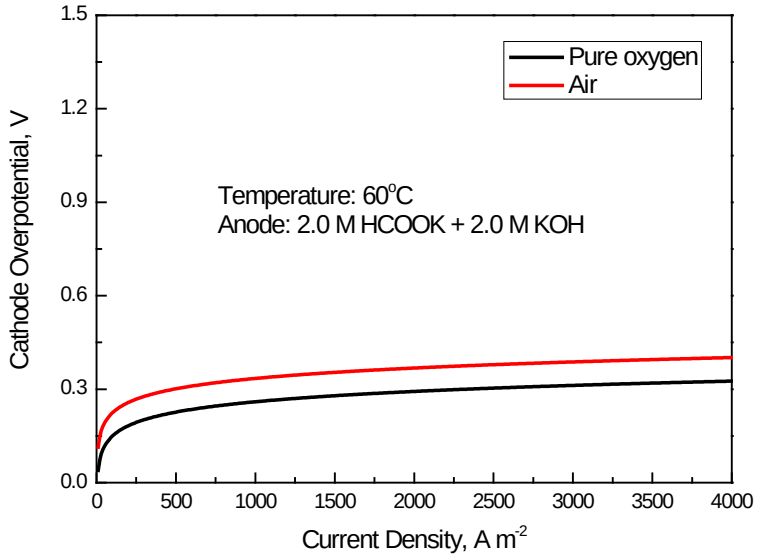

533

534 (b)

535 Fig. 6 Effect of the oxygen concentration on the cell performance: (a) polarization curves and (b)

536 cathode overpotentials.

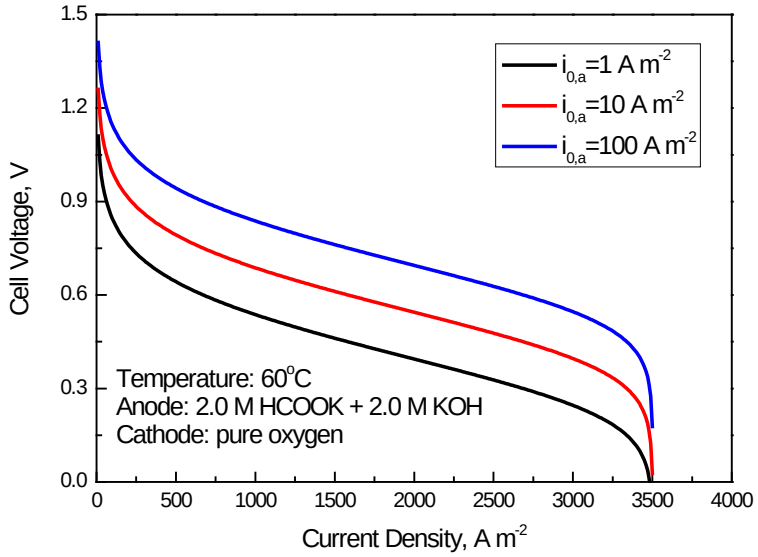

(a)

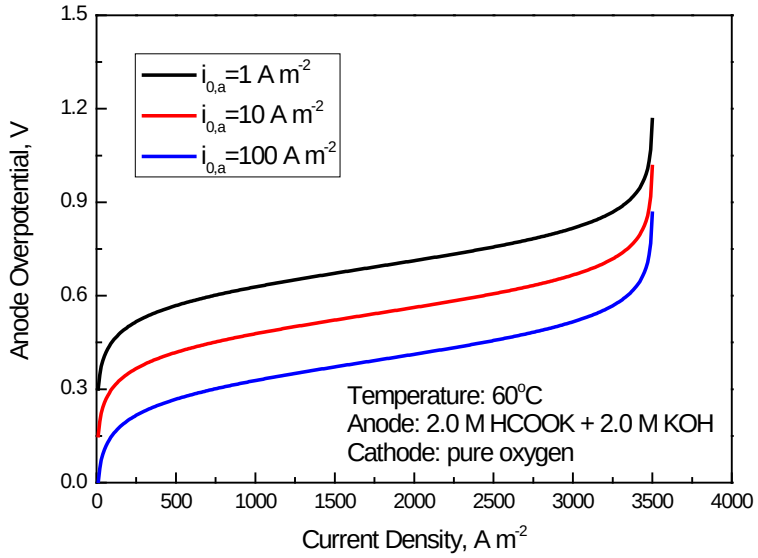

(b)

Fig. 7 Effect of the anodic exchange current density on the cell performance: (a) polarization curves and (b) anode overpotentials.

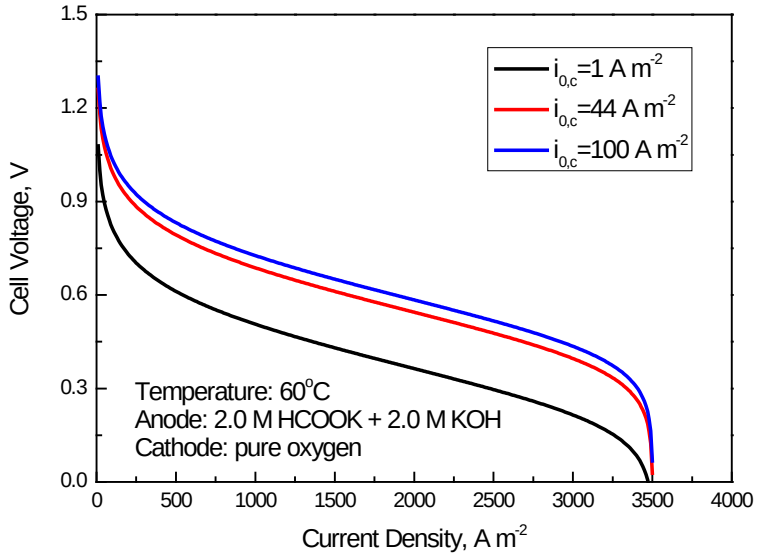

(a)

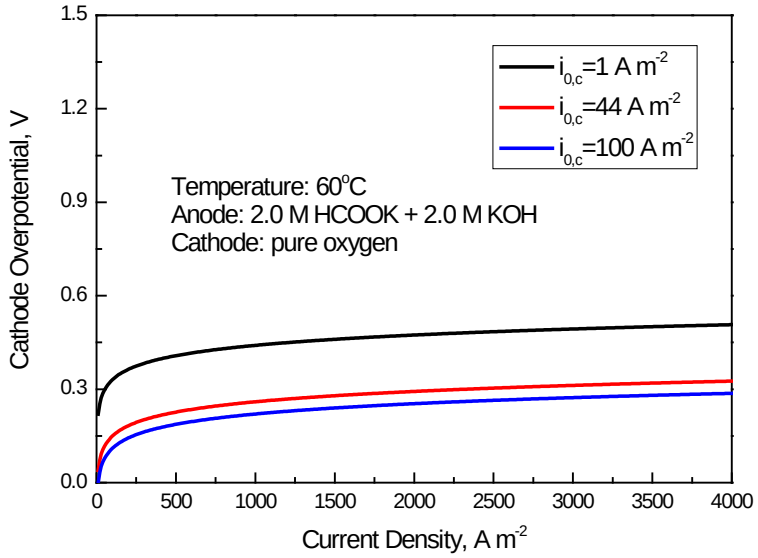

(b)

Fig. 8 Effect of the cathodic exchange current density on the cell performance: (a) polarization curves and (b) anode overpotentials.

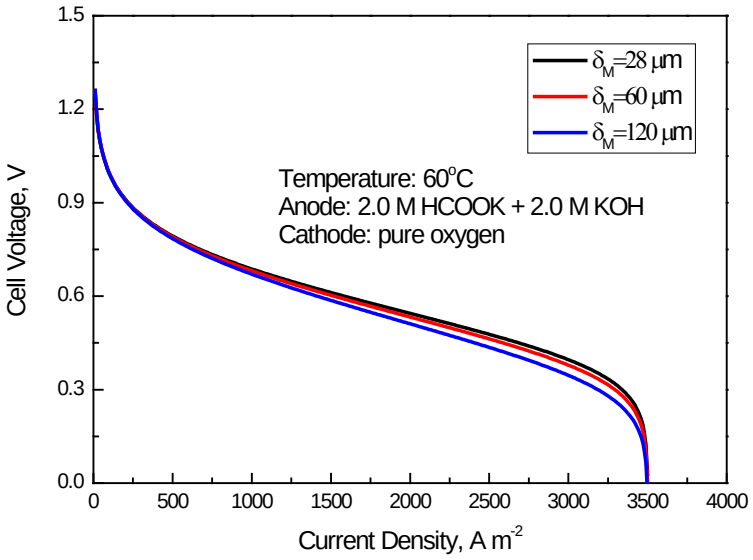

Fig. 9 Effect of the membrane thickness on the cell performance.

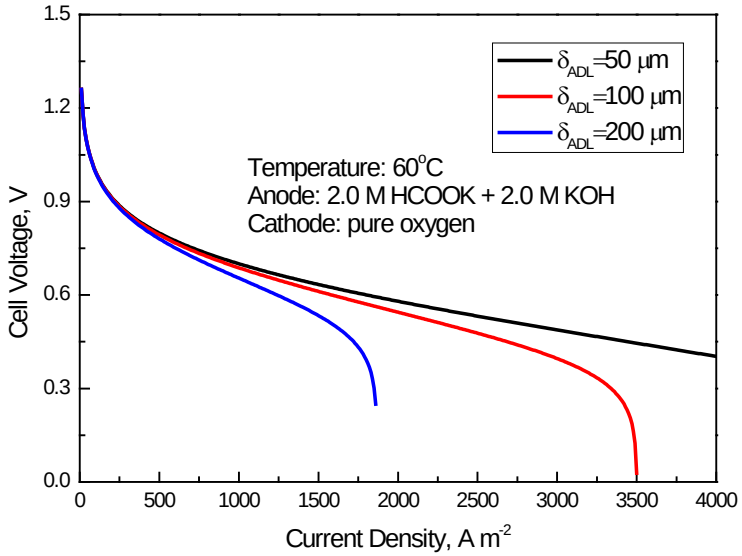

564

565 (a)

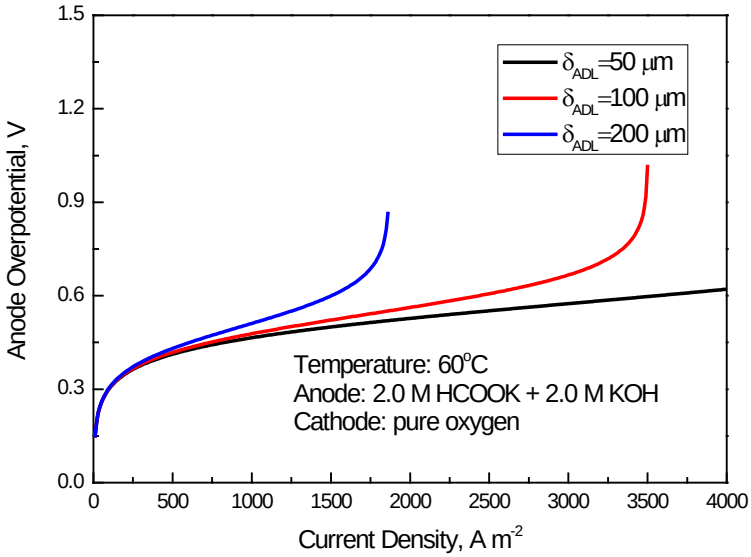

566

567 (b)

568 Fig. 10 Effect of the anode DL thickness on the cell performance: (a) polarization curves and (b)

569 anode overpotentials.

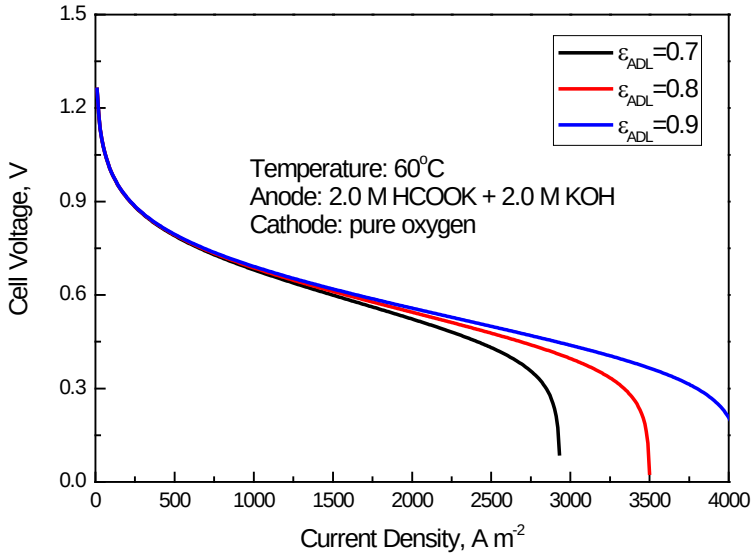

570

571 (a)

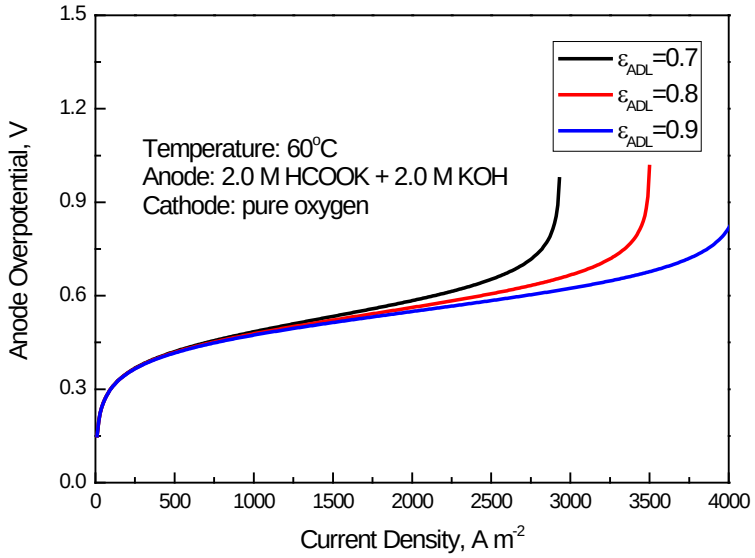

572

573 (b)

574 Fig. 11 Effect of the anode DL porosity on the cell performance: (a) polarization curves and (b)

575 anode overpotentials.

576

Highlights

- A mathematical model is developed for direct formate fuel cells.
- The numerical results are in good agreement with the experimental data.
- The coupled transport and electrochemical processes are incorporated.
- Effects of design and operating parameters on the performance are examined.

Graphical Abstract: A mathmatical model is developed for direct formate fuel cells, which incorporates transport and electrochemical processes.

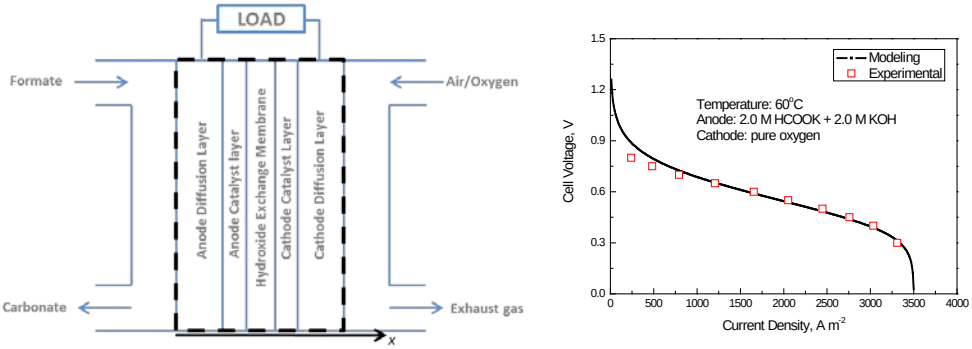

Parameter	Symbol	Value	Unit	Ref.
Anode standard potential	E_0^a	-1.05	V	[26]
Cathode standard potential	E_0^c	0.40	V	[27]
Anode transfer coefficient	α_a	0.44	-	Assumed
Cathode transfer coefficient	α_c	0.5	-	[31]
Anode exchange current density	$i_{0,a}$	10	A m^{-2}	[41]

Cathode exchange current density	$i_{0,c}$	44	A m^{-2}	[42]
Universal gas constant	R	8.314	J mol^{-1} K^{-1}	
Faraday's constant	F	96485.3	A s mol^{-1}	
Number of anode transferred electrons	n_a	2	-	
Number of cathode transferred electrons	n_c	4	-	

590

591 Table 1 Physicochemical parameters.

592

593

594

595

596

597

598

599

600

Parameter	Symbol	Value	Unit	Ref.
Operating temperature	T	333.15	K	
Gas pressure	P	1.013×10^{-5}	Pa	
CO_3^{2-} concentration at inlet	$C_{CO_3^{2-}}^{inlet}$	0	mol m^{-3}	Assumed
O_2 concentration at inlet (air)	$C_{O_2,air}^{inlet}$	$0.21 \times P/(RT)$	mol m^{-3}	[33]
O_2 concentration at inlet (pure O_2)	$C_{O_2,pure}^{inlet}$	$P/(RT)$	mol m^{-3}	[33]

Reference O_2 concentration	$C_{O_2}^{ref}$	$P/(RT)$	mol m^{-3}	[33]
Reference $HCOO^-$ concentration	$C_{HCOO^-}^{ref}$	2000	mol m^{-3}	[38]
Reference OH^- concentration	$C_{OH^-}^{ref}$	2000	mol m^{-3}	[38]

601

602 Table 2 Operating parameters.

603

604

605

606

607

608

609

610

611

612

613

614

Parameter	Symbol	Value	Unit	Ref.
Porosity of anode DL	ε_{ADL}	0.8	-	[43]
Thickness of anode DL	δ_{ADL}	1.0×10^{-4}	m	Estimated
Thickness of membrane	δ_M	2.8×10^{-5}	m	[20]
Porosity of cathode DL	ε_{CDL}	0.8	-	[43]

Thickness of cathode DL	δ_{CDL}	2.0×10^{-4}	m	[44]
Contact resistance	$R_{contact}$	2.0×10^{-5}	$\Omega\ m^2$	[31]

615

616 Table 3 Structural parameters.

617

618

619

620

621

622

623

624

625

626

627

628

629

Parameter	Symbol	Value	Unit	Ref.
Diffusivity of K^+	D_{K^+}	1.96×10^{-9}	$m^2\ s^{-1}$	[45]
Diffusivity of OH^-	D_{OH^-}	5.27×10^{-9}	$m^2\ s^{-1}$	[45]
Diffusivity of CO_3^{2-}	$D_{CO_3^{2-}}$	0.92×10^{-9}	$m^2\ s^{-1}$	[45]
Diffusivity of $HCOO^-$	D_{HCOO^-}	1.45×10^{-9}	$m^2\ s^{-1}$	[45]

Diffusivity of O_2	$D_{O_2,air}$	$1.775\times10^{-5}\times(T/273.15)^{1.823}$	$m^2\ s^{-1}$	[38]
Conductivity of membrane	σ_M	5.5	$\Omega^{-1}\ m^{-1}$	[22]

630

631 Table 4 Mass/charge transport parameters.

632

633